Supplement of Earth Syst. Dynam., 15, 1037–1054, 2024
https://doi.org/10.5194/esd-15-1037-2024-supplement

Earth System Dynamics
Open Access
EGU

Supplement of

Similar North Pacific variability despite suppressed El Niño variability in the warm mid-Pliocene climate

Arthur Merlijn Oldeman et al.

Correspondence to: Arthur Merlijn Oldeman (a.m.oldeman@uu.nl)

Brief description of contents

This supplementary material contains several results in support of the main manuscript. The results presented in the figures (S1 - S9) should be stand-alone with their detailed descriptions in the caption. Below we will provide some additional information for a selection of the results.

Calculating the PDO index

In the main paper we describe how we compute the Niño3.4 index and the Aleutian Low (AL) index. In this Supplement we also briefly treat the Pacific Decadal Oscillation (PDO) index and its correlation with the AL and Niño3.4. The PDO is studied through the dominant principal component (PC) of SST anomalies in the North Pacific (20°N - 70°N, Newman et al. (2003)). The present-day ENSO leads PDO variability and we focus on PDO variability in FMA. These months are chosen because the ocean response can take $\sim$ 1-3 months (e.g. Trenberth and Hurrell, 1994; Newman et al., 2016). We test whether this assumption is valid by computing the lead-lag correlations between ENSO and the AL and PDO time-series, and find that ENSO (and AL) lead PDO with 2-3 months lag with strongest correlations around January Niño3.4, for NOAA observations and the majority of the models (Figures S1 and S9).

Omitting three PlioMIP2 models

In the methods section of the main manuscript we explain that we do not use the results of IPSL-CM6A, MIROC4m and MRI-CGCM2.3 in this study because they do not accurately represent the ENSO - Aleutian low connection in their pre-industrial (E280) reference simulation. Figure S1 shows the monthly lead-lag correlation between the Niño3.4 and AL indices for all models. Based on the NOAA observations, we expect a significant correlation in winter-spring with ENSO leading AL variability. Most models capture this. IPSL-CM6A, MIROC4m and MRI-CGCM2.3 all do not simulate any significant correlation in any relevant combination of months in the pre-industrial. In addition, figure S2 shows the spatial correlation of the DJF Nino index with the DJFM sea-level pressures in the North Pacific. From NOAA observations, we expect a significant correlation in most of the Aleutian low region, and most models capture that (only multi-model mean shown). IPSL-CM6A, MIROC4m and MRI-CGCM2.3 all do not simulate the expected spatial pattern (very little significance in the wrong parts of the AL region). Lastly, figure S3 shows the linear regressions between the DJF Nino index and DJFM AL index. MRI-CGCM2.3 shows a positive correlation which is not correct. IPSL-CM6A and MIROC4m show a weak negative correlation, which is (surprisingly) just statistically significant (p-value $\sim$ 0.04). Considering the regression, the spatial correlations and the lag-correlation, we are not convinced that IPSL-CM6A, MIROC4m and MRI-CGCM2.3 simulate a correct ENSO - AL connection in the pre-industrial, and so we decided to omit them in the main analysis.

Ensemble correlations with the change in residual AL variability

In figure S6 and S7 we show ensemble correlations of the change in the residual AL variability as a function of different changes in the tropics and higher latitudes that could be relevant. Change is defined as mid-Pliocene with regards to pre-industrial (Eoi400 - E280). Figure

S6 shows the ensemble correlations of the change in the residual AL variability with the change in residual West-Equatorial Pacific (WEP) precipitation inf DJF. Residual WEP precipitation has been computed following the same LRM as the residual AL variability. This ensemble correlation is not statistically significant. Changes included in figure S7 are:

- the relative change in sea-ice extent (SIE) in the Arctic in the winter months (DJF), in %, from De Nooijer et al. (2020);
- the absolute change in sea-surface temperatures (SST) averaged in the AL region in DJF, in °C (this study);
- the absolute change in annual mean strength of the Atlantic Meridional Overturning Circulation (AMOC), in Sv, from Weiffenbach et al. (2023);
- and the absolute change in annual mean surface air temperatures (SAT) averaged over the Arctic, in °C, from De Nooijer et al. (2020).

Figure S7 shows that not one of these changes is able to explain the AL residual change alone throughout the PlioMIP2 ensemble. It doesn't mean that none of these changes are able to explain the change in residual AL variability in one individual model.

Ensemble correlations of changes in the tropical Pacific

In Figure S8 we include ensemble correlations between three changes in variables that are relevant for the summary view presented in the main manuscript Figure 8. From literature, we find that, according to the PlioMIP2 ensemble mean and the majority of the models, the Indian Ocean warms more than the West Pacific Ocean (Ren et al., 2023), that the rising branch of the Pacific Walker circulation (PWC) moves westward both in the annual mean and in winter (Han et al., 2021; Zhang et al., 2024), and that El Niño variability is suppressed (Oldeman et al., 2021; Pontes et al., 2022). The results in Figure S8 show that the amplitudes of these changes are related through to the PlioMIP2 ensemble. The change in ENSO amplitude is defined as following the main manuscript. The central longitude of the PWC is obtained via Zixuan Han (as calculated in Han et al., 2021), where negative means westward. The West Pacific - Indian Ocean SST gradient is calculated as the difference between SSTs averaged in 130°E-180° (West Pacific) and 40°E-90°E (Indian Ocean), both between 10°S and 15°N.

References

De Nooijer, W., Zhang, Q., Li, Q., Zhang, Q., Li, X., Zhang, Z., Guo, C., Nisancioglu, K. H., Haywood, A. M., Tindall, J. C., Hunter, S. J., Dowsett, H. J., Stepanek, C., Lohmann, G., Otto-Bliesner, B. L., Feng, R., Sohl, L. E., Chandler, M. A., Tan, N., Contoux, C., Ramstein, G., Baatsen, M. L., Von Der Heydt, A. S., Chandan, D., Peltier, W. R., Abe-Ouchi, A., Chan, W. L., Kamae, Y., and Brierley, C. M. (2020). Evaluation of Arctic warming in mid-Pliocene climate simulations. *Climate of the Past*, 16(6):2325–2341.

Han, Z., Zhang, Q., Li, Q., Feng, R., Haywood, A. M., Tindall, J. C., Hunter, S. J., Otto-Bliesner, B. L., Brady, E. C., Rosenbloom, N., Zhang, Z., Li, X., Guo, C., Nisancioglu, K. H., Stepanek, C., Lohmann, G., Sohl, L. E., Chandler, M. A., Tan, N., Ramstein, G., Baatsen, M. L. J., von der Heydt, A. S., Chandan, D., Peltier, W. R., Williams, C. J. R., Lunt, D. J., Cheng, J.,

Wen, Q., and Burls, N. J. (2021). Evaluating the large-scale hydrological cycle response within the Pliocene Model Intercomparison Project Phase 2 (PlioMIP2) ensemble. *Climate of the Past*, 17(6):2537–2558.

Newman, M., Alexander, M. A., Ault, T. R., Cobb, K. M., Deser, C., Di Lorenzo, E., Mantua, N. J., Miller, A. J., Minobe, S., Nakamura, H., Schneider, N., Vimont, D. J., Phillips, A. S., Scott, J. D., and Smith, C. A. (2016). The Pacific Decadal Oscillation, Revisited. *Journal of Climate*, 29(12):4399–4427.

Newman, M., Compo, G. P., and Alexander, M. A. (2003). ENSO-forced variability of the Pacific decadal oscillation. *Journal of Climate*, 16(23):3853–3857.

Oldeman, A. M., Baatsen, M. L. J., von der Heydt, A. S., Dijkstra, H. A., Tindall, J. C., Abe-Ouchi, A., Booth, A. R., Brady, E. C., Chan, W.-L., Chandan, D., Chandler, M. A., Contoux, C., Feng, R., Guo, C., Haywood, A. M., Hunter, S. J., Kamae, Y., Li, Q., Li, X., Lohmann, G., Lunt, D. J., Nisancioglu, K. H., Otto-Bliesner, B. L., Peltier, W. R., Pontes, G. M., Ramstein, G., Sohl, L. E., Stepanek, C., Tan, N., Zhang, Q., Zhang, Z., Wainer, I., and Williams, C. J. R. (2021). Reduced El Niño variability in the mid-Pliocene according to the PlioMIP2 ensemble. *Climate of the Past*, 17(6):2427–2450.

Pontes, G. M., Taschetto, A. S., Sen Gupta, A., Santoso, A., Wainer, I., Haywood, A. M., Chan, W.-L., Abe-Ouchi, A., Stepanek, C., Lohmann, G., Hunter, S. J., Tindall, J. C., Chandler, M. A., Sohl, L. E., Peltier, W. R., Chandan, D., Kamae, Y., Nisancioglu, K. H., Zhang, Z., Contoux, C., Tan, N., Zhang, Q., Otto-Bliesner, B. L., Brady, E. C., Feng, R., von der Heydt, A. S., Baatsen, M. L. J., and Oldeman, A. M. (2022). Mid-Pliocene El Niño/Southern Oscillation suppressed by Pacific intertropical convergence zone shift. *Nature Geoscience*, 15:726–734.

Ren, X., Lunt, D. J., Hendy, E., Williams, C. J. R., Stepanek, C., Guo, C., Chandan, D., Lohmann, G., Tindall, J. C., Sohl, L. E., Chandler, M. A., Kageyama, M., Baatsen, M. L. J., Tan, N., Zhang, Q., Feng, R., Hunter, S., Chan, W.-L., Peltier, W. R., Li, X., Kamae, Y., Zhang, Z., and Haywood, A. M. (2023). The hydrological cycle and ocean circulation of the Maritime Continent in the Pliocene: results from PlioMIP2. *Climate of The Past*.

Trenberth, K. E. and Hurrell, J. W. (1994). Decadal atmosphere-ocean variations in the Pacific. *Climate Dynamics*.

Weiffenbach, J. E., Baatsen, M. L. J., Dijkstra, H. A., von der Heydt, A. S., Abe-Ouchi, A., Brady, E. C., Chan, W.-L., Chandan, D., Chandler, M. A., Contoux, C., Feng, R., Guo, C., Han, Z., Haywood, A. M., Li, Q., Li, X., Lohmann, G., Lunt, D. J., Nisancioglu, K. H., Otto-Bliesner, B. L., Peltier, W. R., Ramstein, G., Sohl, L. E., Stepanek, C., Tan, N., Tindall, J. C., Williams, C. J. R., Zhang, Q., and Zhang, Z. (2023). Unraveling the mechanisms and implications of a stronger mid-Pliocene Atlantic Meridional Overturning Circulation (AMOC) in PlioMIP2. *Climate of the Past*, 19(1):61–85.

Zhang, K., Sun, Y., Zhang, Z., Stepanek, C., Feng, R., Hill, D., Lohmann, G., Dolan, A., Haywood, A., Abe-Ouchi, A., Otto-Bliesner, B., Contoux, C., Chandan, D., Ramstein, G., Dowsett, H., Tindall, J., Baatsen, M., Tan, N., Peltier, W. R., Li, Q., Chan, W.-L., Wang, X., and Zhang, X. (2024). Revisiting the physical processes controlling the tropical atmospheric circulation changes during the Mid-Piacenzian Warm Period. *Quaternary International*, page S1040618224000016.

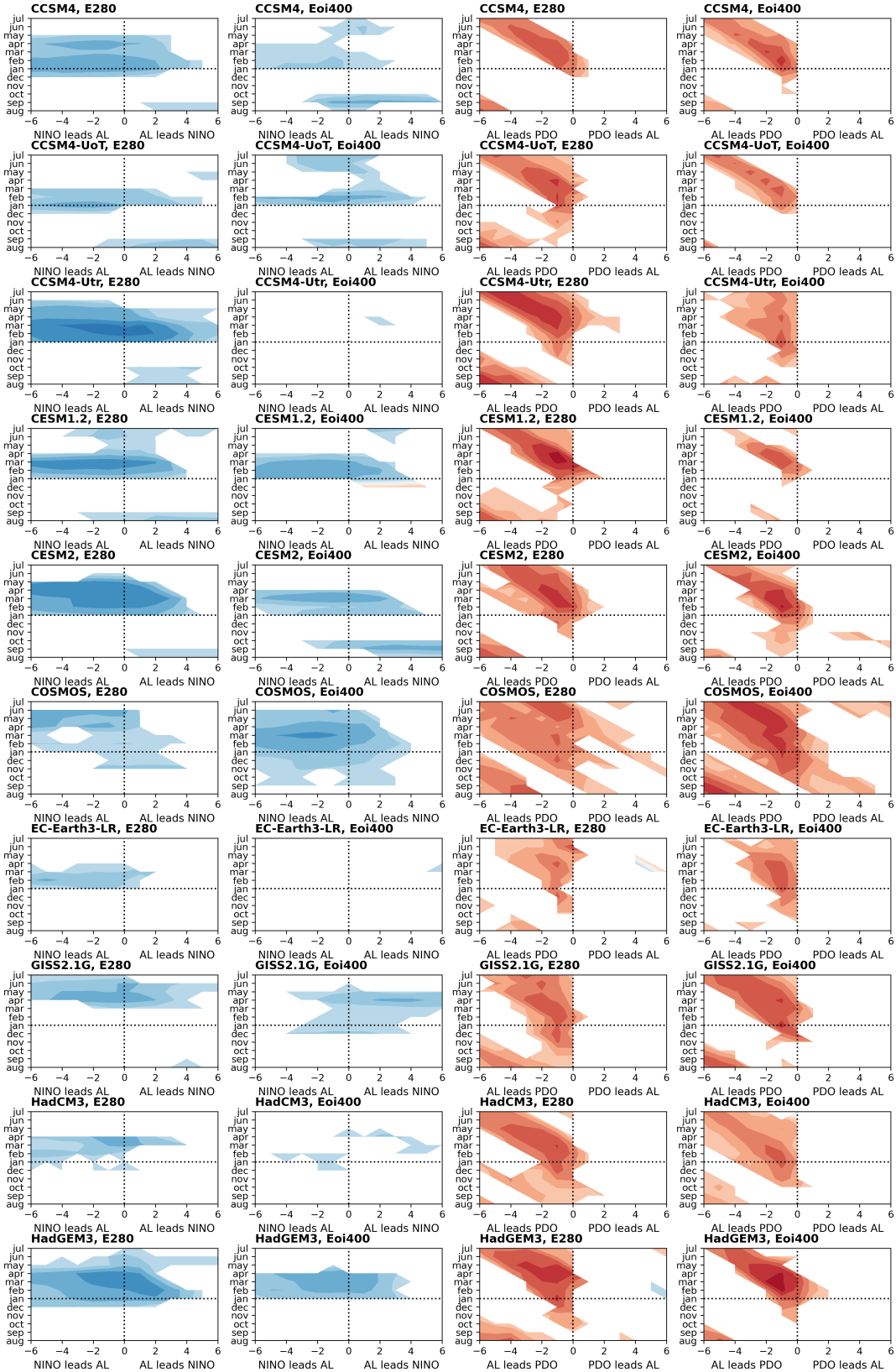

Figure S1: Lag-correlations for monthly Niño3.4 with Aleutian low (AL) index (left two panels) and for AL index with PDO index (right two panels), both for pre-industrial reference (E280) and mid-Pliocene (Eoi400) simulations, for all models, including multi-model mean and NOAA result. Correlation coefficients only shown when statistically significant (p-value<0.05). Figure continues on the next page.

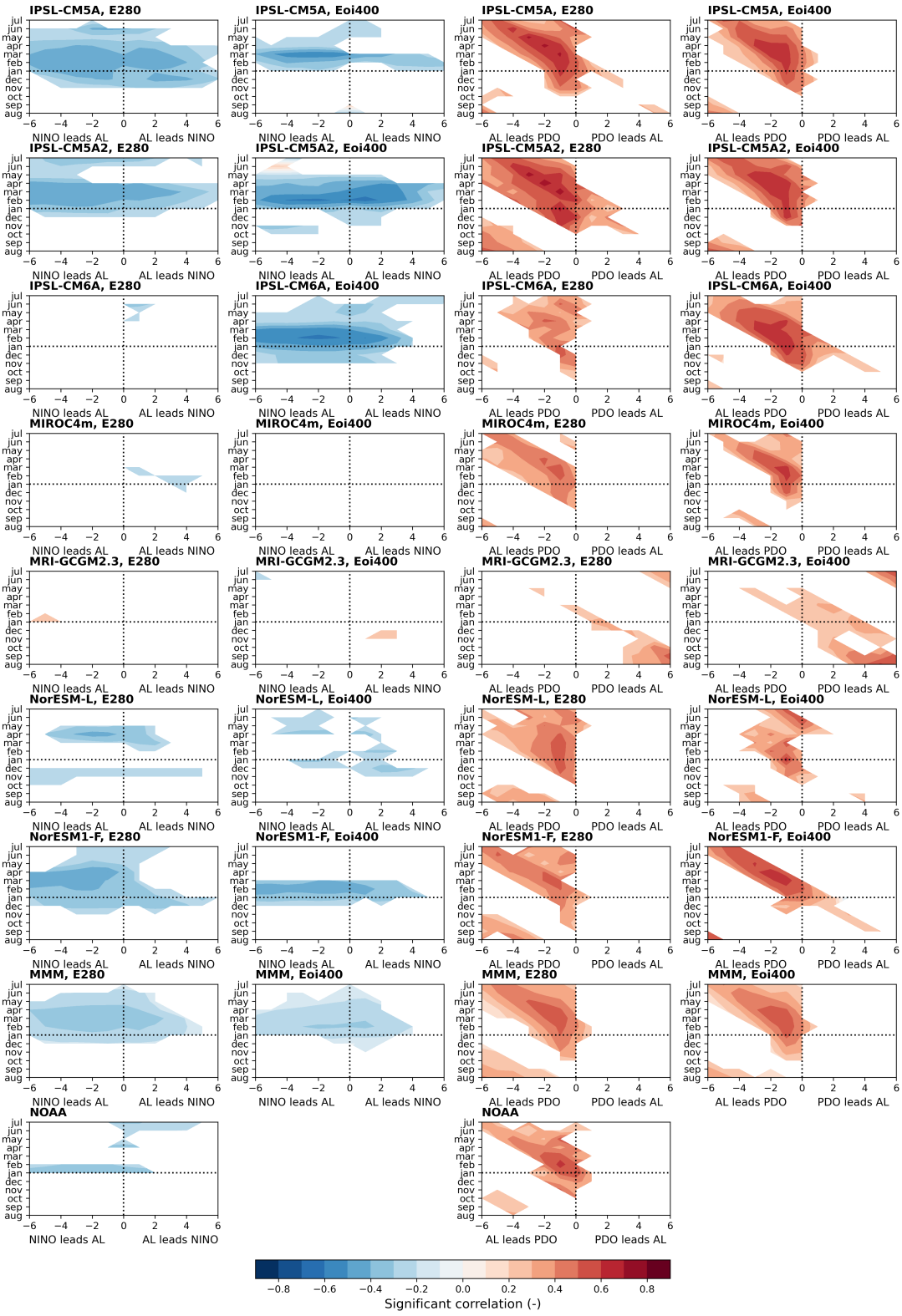

Figure S1, continued: Lag-correlations for Niño3.4 with Aleutian low (AL) index (left two panels) and for AL index with PDO index (right two panels), both for pre-industrial reference (E280) and mid-Pliocene (Eoi400) simulations, for all models, including multi-model mean and NOAA result. Correlation coefficients only shown when statistically significant (p-value<0.05).

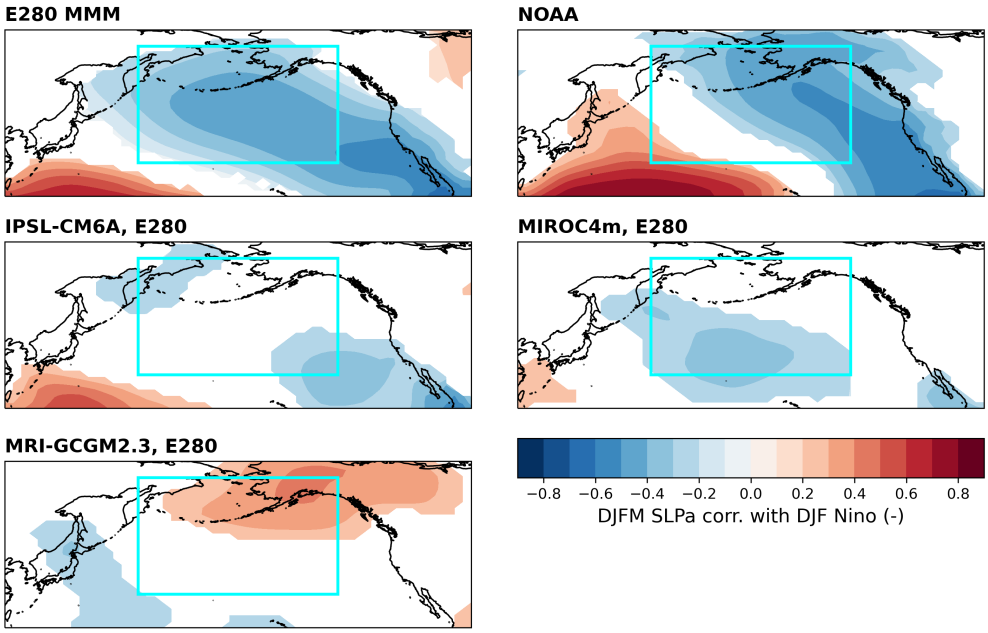

Figure S2: Correlation maps of the DJF Niño3.4 index with DJFM sea-level pressure (SLP) anomalies. For the E280 multi-model mean (MMM), NOAA observations, and pre-industrial IPSL-CM6A, MIROC4m and MRI-CGCM2.3. Correlation only shown when statistically significant (p-value<0.05). Cyan box drawn is the Aleutian low region (index reference).

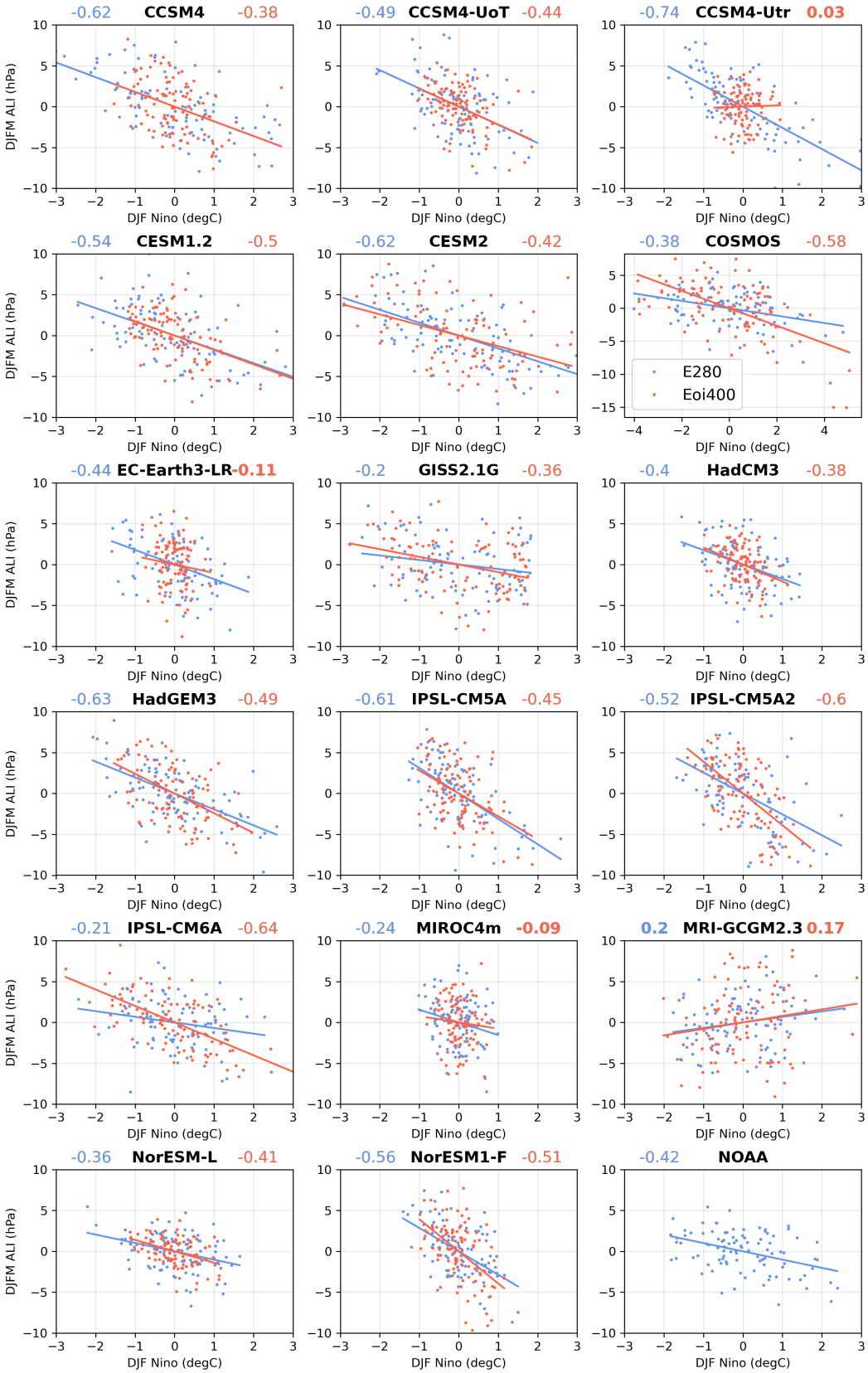

Figure S3: Scatter plots of DJF Niño3.4 index vs DJFM AL index, for all models and simulations, including NOAA. Pre-industrial in blue, mid-Pliocene in red. Including a linear fit or regression. Correlation coefficients included in plot titles, in **bold** when the correlation is positive or not statistically significant (i.e. when p-value>0.05). Note different axes limits for COSMOS only.

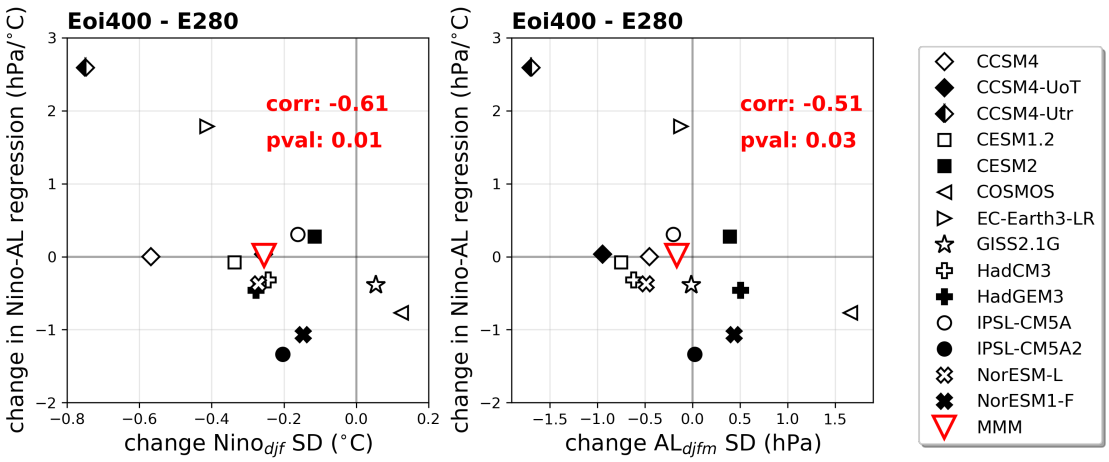

Figure S4: Change (Eoi400 - E280) in the ENSO - AL regression as a function of (left) change in the ENSO amplitude (defined as DJF Niño3.4 SD) and (right) change in the AL amplitude (defined as DJFM AL index SD). Plots include ensemble correlation and p-value.

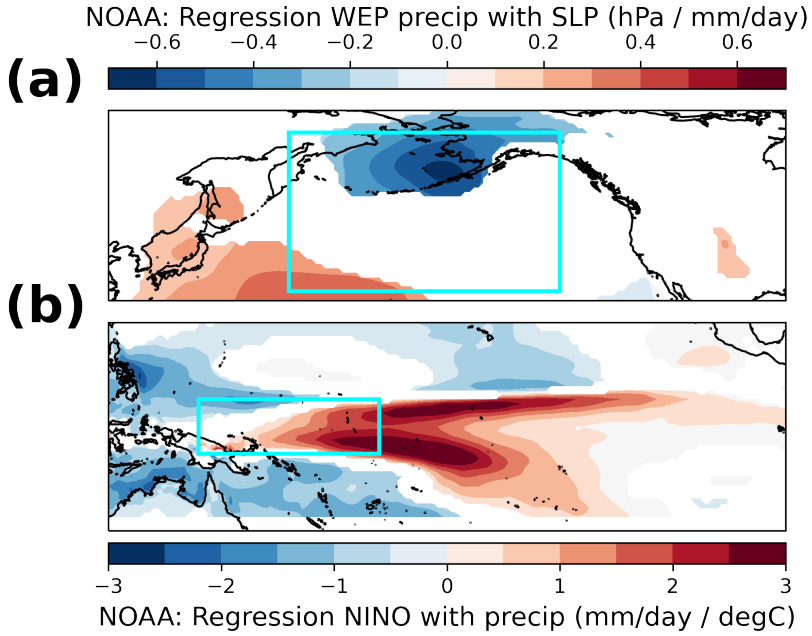

Figure S5: NOAA regression between (a) DJF precipitation in the west-equatorial Pacific (WEP) and DJFM SLP in the North Pacific. Cyan rectangle indicates Aleutian low region. And (b) between DJF Niño3.4 index and DJF precipitation. Cyan rectangle indicates WEP region. Regressions are only shown if the correlation is statistical significant (p-value<0.05).

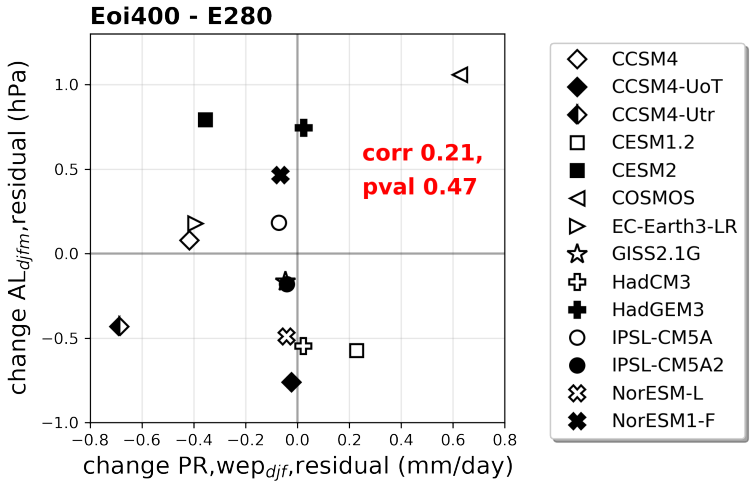

Figure S6: Change (Eoi400 - E280) in the residual DJFM AL variability (i.e. the part of the variability that is not linearly correlated to ENSO) as a function of the change in the residual DJF precipitation in the West-Equatorial Pacific (WEP). Residual WEP precipitation has been computed following the LRM as explained in the main paper.

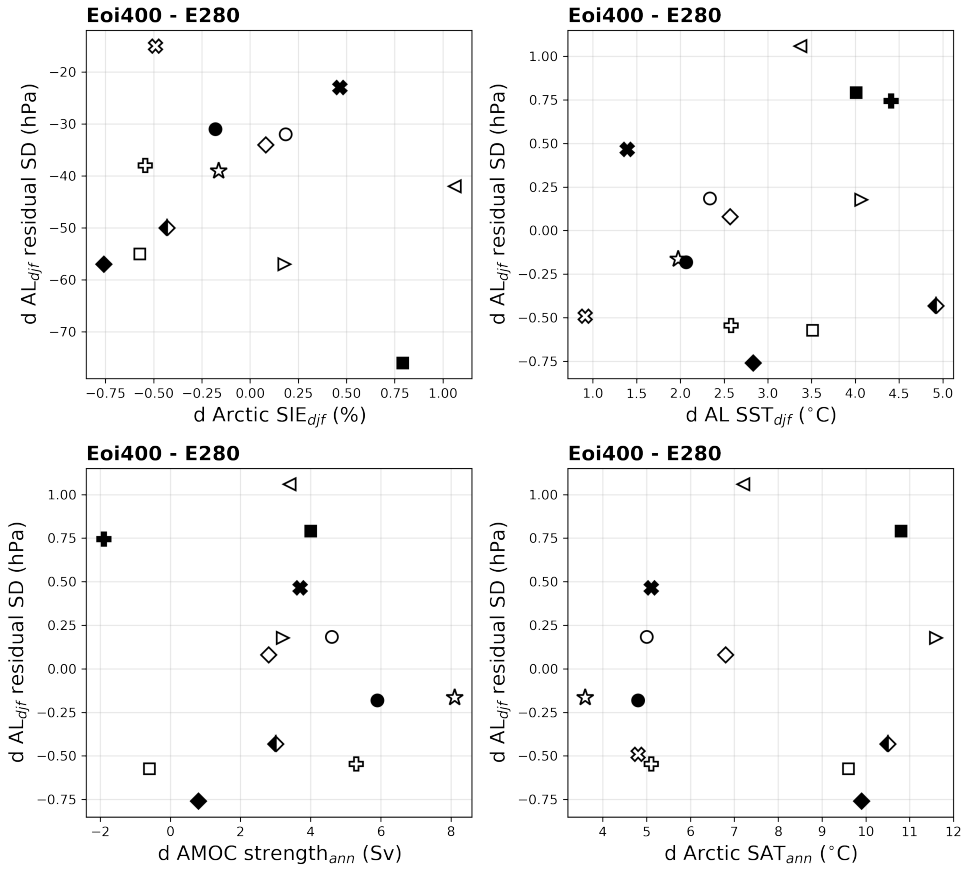

Figure S7: Change (Eoi400 - E280) in the residual DJFM AL variability (i.e. the part of the variability that is not linearly correlated to ENSO) as a function of: (top left) relative change in Arctic sea-ice extext in DJF (SIE); (top right) absolute change in sea-surface temperatures (SST) averaged in the AL region in DJF; (bottom left) absolute change in annual mean AMOC strength; and (bottom right) absolute change in annual mean Arctic surface air temperatures (SAT). None of the ensemble scatters show a significant correlation.

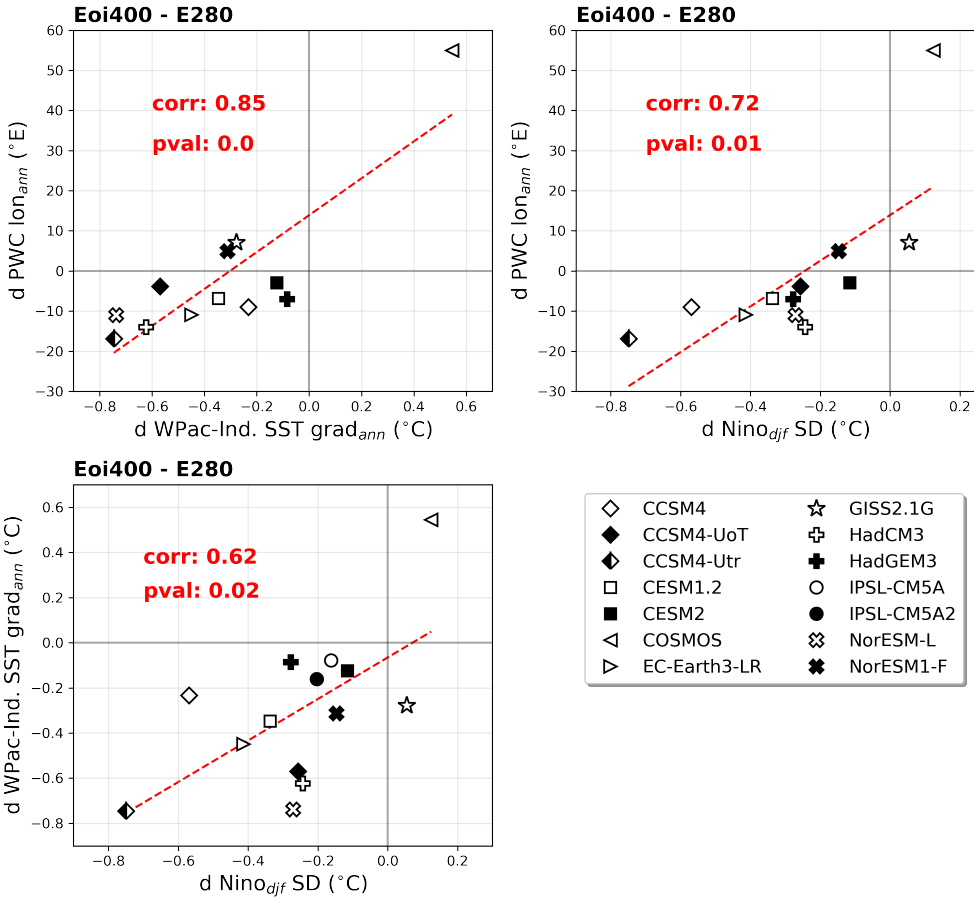

Figure S8: Scatter plots of three changes between the mid-Pliocene and pre-industrial simulations (Eoi400 - E280). Change in the central longitude of the Pacific Walker circulation (PWC) in the annual mean (d PWC lon), Change in the SST difference between the tropical West Pacific Ocean and Indian Ocean in the annual mean (d Indo-Pac SST grad), and Change in the winter ENSO amplitude (d Nino SD). The three scatter plots show the three possible combinations of two of these changes. All combinations between these variables yield a significant ensemble correlation.

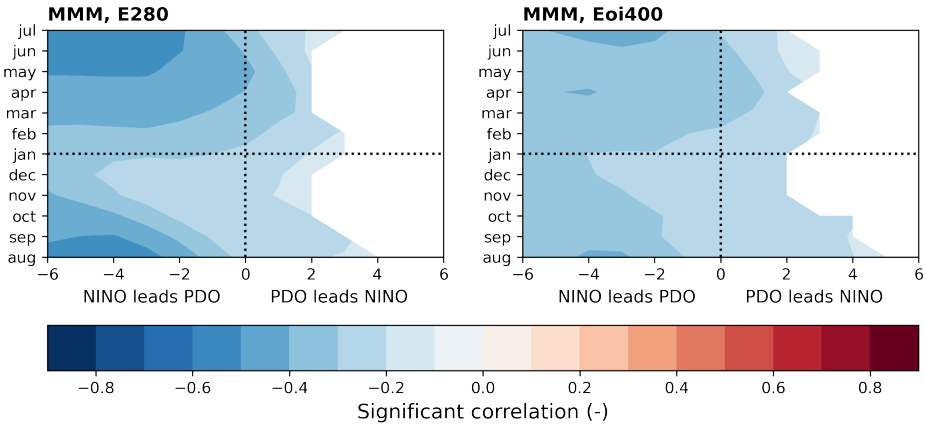

Figure S9: Multi model mean lag-correlations for monthly Niño3.4 with PDO index, both for pre-industrial reference (E280, left) and mid-Pliocene (Eoi400, right) simulations. Correlation coefficients only shown when statistically significant (p-value<0.05) for more than 6 models.